

## Hypoxia-tolerant zooplankton may reduce biological carbon pump efficiency in the Humboldt current system off Peru

Anja Engel <sup>1✉</sup>, Carolina Cisternas-Novoa<sup>1,2</sup>, Helena Hauss <sup>1,3</sup>, Rainer Kiko<sup>1,4</sup> & Frédéric A. C. Le Moigne<sup>1,5</sup>

In the ocean, downward flux of particles produced in sunlit surface waters is the major component of the biological carbon pump, which sequesters atmospheric carbon dioxide and fuels deep-sea ecosystems. The efficiency of downward carbon transfer is expected to be particularly high in tropical upwelling systems where hypoxia occurring beneath the productive surface waters is thought to hamper particle consumption. However, observations of both particle feeders and carbon export in low-oxygen waters are scarce. Here, we provide evidence that hypoxia-tolerant zooplankton feed on sinking particles in the extensive Oxygen Minimum Zone (OMZ) off Peru. Using several arrays of drifting sediment traps and in situ imaging, we show geochemical and morphological transformations of sinking particles and substantial control of carbon export by zooplankton. Our findings challenge the assumption of a consistently efficient biological carbon pump in OMZs and further demonstrate the need to consider mesopelagic organisms when studying oceanic carbon sequestration.

<sup>1</sup>GEOMAR, Helmholtz Centre for Ocean Research Kiel, Kiel, Germany. <sup>2</sup>Memorial University, St John's, Newfoundland and Labrador, Canada. <sup>3</sup>NORCE Norwegian Research Centre, Division Climate & Environment, Bergen, Norway. <sup>4</sup>Sorbonne Université, Laboratoire d'Océanographie de Villefranche, Villefranche-sur-Mer, France. <sup>5</sup>Univ. Brest, CNRS, IRD, Ifremer, LEMAR, France. ✉email: [aengel@geomar.de](mailto:aengel@geomar.de)

The biological carbon pump (BCP) sequesters CO<sub>2</sub> from the ocean's surface to the deep sea<sup>1</sup>, mitigating increasing atmospheric CO<sub>2</sub> concentrations<sup>2</sup>. The storage time of carbon entering the dark ocean via the BCP depends on the depth at which organic matter is remineralized back to CO<sub>2</sub>. The shallower the remineralization depth, the faster the CO<sub>2</sub> will eventually escape into the atmosphere<sup>3</sup>. Climate change induced by variability in atmospheric CO<sub>2</sub> concentration also relates to changes in the efficiency of the BCP (BCP<sub>eff</sub>)<sup>4</sup>, being a function of both the carbon export efficiency ( $E_{\text{eff}}$ ) and the carbon transfer efficiency ( $T_{\text{eff}}$ ):

$$\text{BCP}_{\text{eff}} = E_{\text{eff}} \times T_{\text{eff}} \quad (1)$$

$$E_{\text{eff}} = \frac{F_{z0}}{\text{PP}} \quad (2)$$

$$T_{\text{eff}} = \frac{F_z}{F_{z0}} \quad (3)$$

where  $F_{z0}$  is the particulate organic carbon (POC) export flux out of the surface ocean, PP is the amount of CO<sub>2</sub> fixed by primary production and ( $F_z$ ) is the POC flux at a particular depth  $z$ .  $T_{\text{eff}}$  is related to the attenuation of particle flux, often characterized as the exponent  $b$  of the *Martin* power-law function<sup>5</sup>:

$$F_z = F_{100} \times \left(\frac{z}{100}\right)^{-b} \quad (4)$$

with 100 being the standard reference depth (m) for  $F_{z0}$ . A higher *Martin*  $b$  coefficient means stronger flux attenuation and less efficient downward transport of carbon. BCP<sub>eff</sub> is controlled by multiple factors influencing  $E_{\text{eff}}$ ,  $T_{\text{eff}}$ , or both, such as plankton growth, species diversity, particle sinking velocity, zooplankton feeding, and microbial remineralization<sup>6,7</sup>.

As a consequence of climate change, the ocean is losing oxygen, leading to an expansion and intensification of OMZs with severe consequences for marine biota and biogeochemical cycles<sup>8</sup>. The largest present-day OMZs are associated with highly productive Eastern Boundary Upwelling Systems, which are responsible for ~25% of carbon export globally<sup>9</sup>. Deoxygenation reduces heterotrophic activity and results in the selection of organisms with little or no metabolic demand for oxygen<sup>10</sup>. To thrive under low oxygen concentration (hypoxia: <60 μmol O<sub>2</sub> L<sup>-1</sup>) or even

complete absence of oxygen (anoxia), microorganisms such as bacteria and archaea use anaerobic respiration pathways<sup>11</sup>. Most zooplankton and nekton species avoid low-oxygen environments, these include many taxa known to feed on or break up sinking particles<sup>12</sup>. Therefore, a widespread assumption is that reduced zooplankton activity in OMZs results in higher  $T_{\text{eff}}$  and, hence, in higher efficiency of the BCP<sup>13–15</sup>. One of the ocean's most extensive and intense permanent OMZ is associated with the Humboldt Current System off Peru and Chile<sup>16</sup>, occupying ~2 × 10<sup>6</sup> km<sup>3</sup>. In this region, several zooplankton species migrate into the OMZ core daily, surviving prolonged oxygen depletion<sup>17–19</sup>. The impact of hypoxia-tolerant particle feeders on the BCP remains unknown. Yet, their interactions with particle flux might challenge the current view<sup>20</sup> that (1) productive regions with a severe OMZ have a high  $T_{\text{eff}}$ , and (2) future expansion of OMZs may enhance CO<sub>2</sub> sequestration overall. Here, we determined  $T_{\text{eff}}$  for the hypoxic waters along the continental margin off Peru. Using surface-tethered sediment traps at 5–8 depths, with the shallowest trap placed below the surface mixed layer (ML) and the euphotic zone (EZ), i.e., 40–60 m, and the deepest trap at ≤600 m, we obtained a high-resolution dataset of export fluxes for the upper mesopelagic zone, where most of the flux attenuation occurs. We combined sediment trap sampling with zooplankton surveys using in situ imaging and Multinet vertical hauls. Based on our results, we argue for a revised view of BCP<sub>eff</sub> in OMZs that explicitly includes zooplankton-induced particle transformation.

## Results and discussion

**Carbon export fluxes and flux attenuation in the OMZ.** We deployed particle interceptor traps six times (T1–T4, T6, T7) at different locations off Peru (12.0°S–14.6°S and 77.3°W–78.6°W; Supplementary Fig. 1) during the *RV METEOR* cruises M136 and M138; four times in April and two times in June 2017 (see Methods; Supplementary Table 1). Phytoplankton abundance in the upper mixed layer varied considerably between the cruises and deployment sites as indicated by chlorophyll-*a* (Chl*a*) concentrations<sup>21</sup> (Supplementary Fig. 1). Chl*a* concentrations were higher in April (avg.: 3.1 ± 2.6, max: 11 μg L<sup>-1</sup>) than in June (avg.: 2.8 ± 1.6, max: 4 μg L<sup>-1</sup>). Oxygen concentrations declined rapidly below 20–50 m water depth and increased again below 500 m (Fig. 1a–f), indicating severe hypoxic conditions

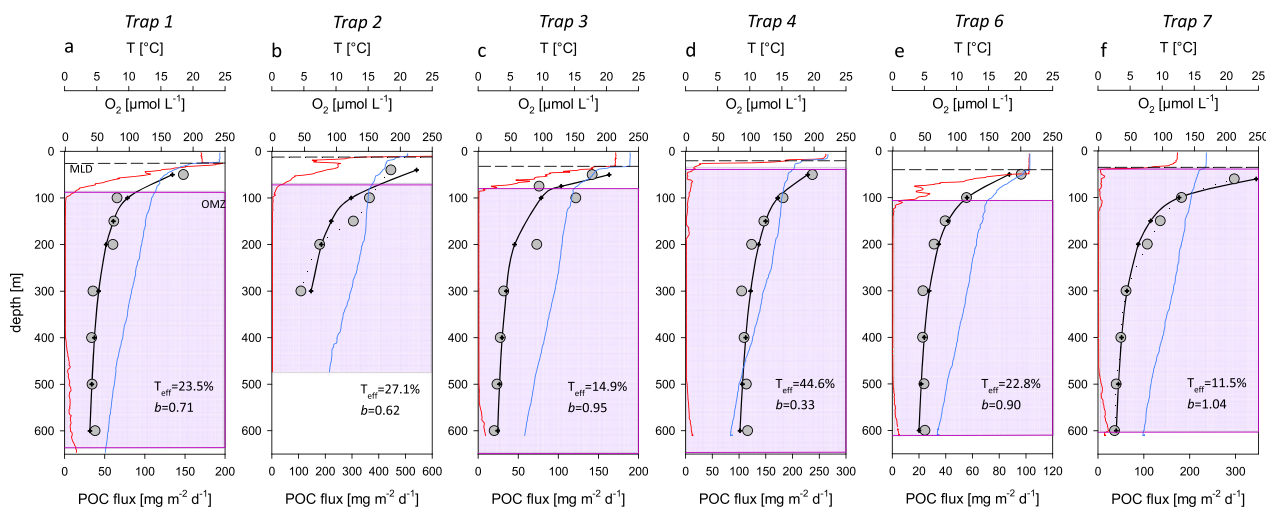


**Fig. 1 Carbon export fluxes off Peru.** a–f Particulate organic carbon (POC) export fluxes (grey circles) were measured using sediment traps; the solid black lines and crosses correspond to regression curves (power law function)<sup>5</sup> fitted to the data with the depth of the shallowest trap as reference depth for fluxes out of the mixed layer ( $F_{z0}$ ). Also shown are temperature (blue) and oxygen concentration (red) profiles, the depth of the mixed layer (MLD; dashed line) and the extent of the OMZ (purple shading; <15 μmol O<sub>2</sub> kg<sup>-1</sup>).

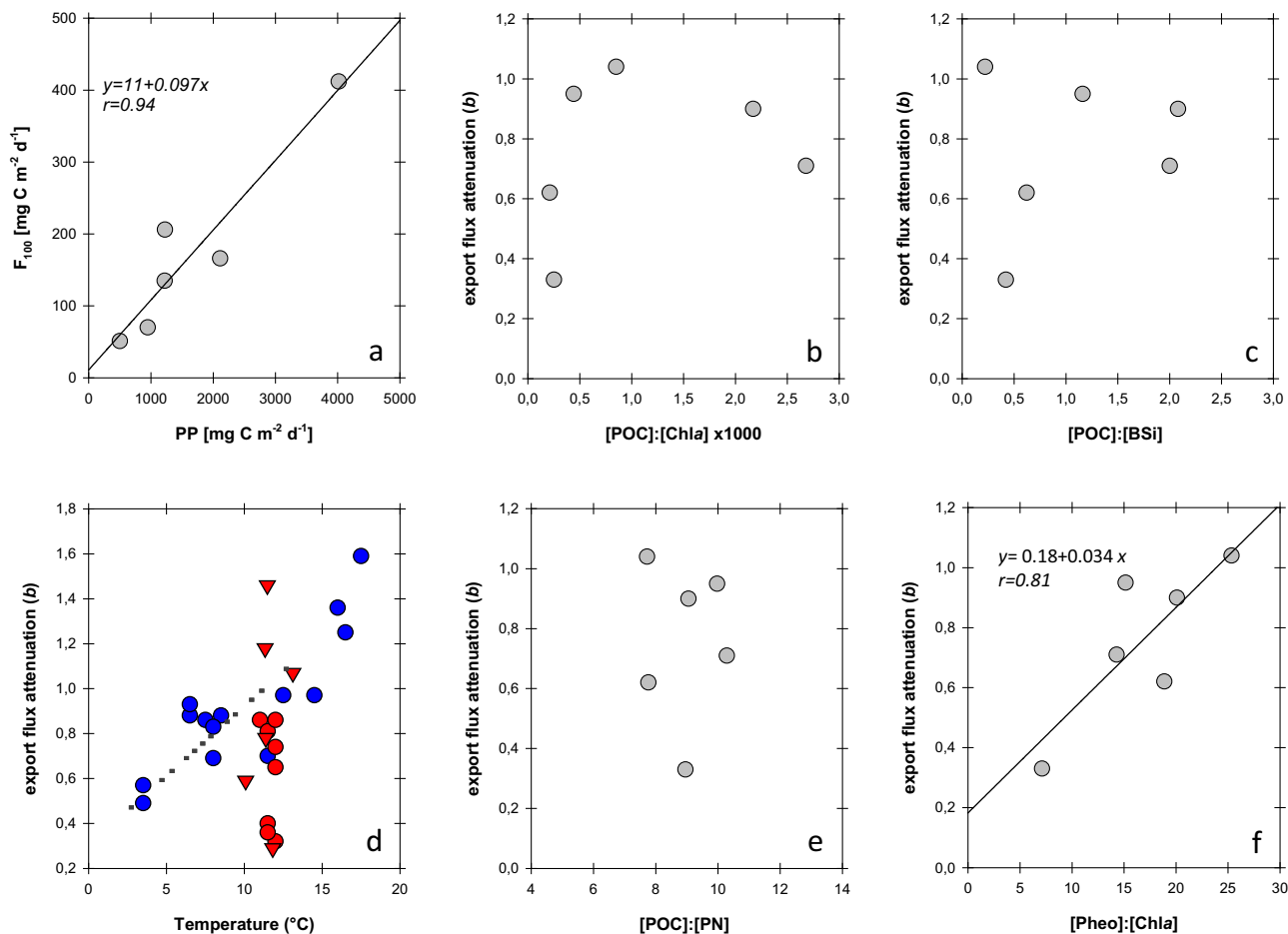


**Fig. 2 Potential drivers of export flux attenuation.** **a** Relationship between carbon export flux and satellite-derived primary production<sup>23</sup> (PP, during the period of deployment); **b, c, e, f** Export flux attenuation coefficient (*Martin-b*) and biochemical parameters indicative of particle quality as obtained in the deepest trap of each deployment. Ratios are [g]:[g] in (**b, c, f**), and [mol]:[mol] in (**e**); and **d** export flux attenuation coefficients and temperature as suggested by Marsay et al.<sup>29</sup> (dotted line). blue symbols: *Martin-b* values from well-oxygenated waters ( $>200 \mu\text{mol L}^{-1}$ ), red symbols: OMZ ( $<70 \mu\text{mol L}^{-1}$ ) with circles: previously published data (Supplementary Table 3), and triangles: data from this study. All *b*-values in **d** were calculated with a reference depth of 100 m for comparison.

( $<15.0 \mu\text{mol O}_2 \text{ L}^{-1}$ )<sup>22</sup> in the upper mesopelagic zone. Temperature declined at shallow depth (20–30 m), indicating a MLD of  $<50$  m, slightly shallower than the EZ depth, which ranged between 25 and 48 m (Supplementary Table 2). Below the MLD, the temperature decreased steadily and within similar ranges at all deployment sites (Fig. 1a–f). All vertical profiles of downward fluxes of POC closely followed the *Martin*-type power-law function (Fig. 1a–f, Supplementary Table 2). Absolute carbon fluxes and flux attenuation in the OMZ differed clearly between the deployment sites. The highest flux at 100 m was recorded on the shelf in April, T2 ( $F_{100} = 412 \text{ mg C m}^{-2} \text{ d}^{-1}$ ), and the lowest for T6 in June ( $F_{100} = 51 \text{ mg C m}^{-2} \text{ d}^{-1}$ ). Overall, carbon export flux ( $F_{100}$ ) was closely related to primary production (PP) ( $r = 0.94$ ,  $p < 0.01$ ), derived from remote sensing data using the vertically generalized productivity model (standard VGPM)<sup>23</sup> (Fig. 2a). Hence, despite large spatial and temporal differences in PP, export efficiency,  $E_{\text{eff}} = \Delta[F_{100}]/\Delta[\text{PP}]$ , was similar for all deployments, indicating that approximately 10% of the PP was exported below the mixed layer.

Since both the ML and EZ were shallow ( $<50$  m) in the study region, we calculated transfer efficiencies ( $T_{\text{eff}}$ ) and attenuation coefficients (*b*-values) using the shallowest trap as reference depth for fluxes out of the surface ocean ( $F_{z0}$ )<sup>4</sup> (Fig. 1a–f). Attenuation

of carbon flux was highest at T7, showing a *Martin-b* of 1.04 and thus the least efficient carbon transfer to depth ( $T_{\text{eff}} = 11.5\%$ ). In contrast,  $T_{\text{eff}}$  at T4 was almost four times higher (44.6%), with a *Martin-b* of 0.33. Regarding all deployments, no significant relationship was observed between  $F_{z0}$  and *Martin-b* values, indicating that the amount of POC exported did not control the flux attenuation within the mesopelagic OMZ. *Martin-b* values at similar deployment sites, i.e., T4 and T6, as well as T1 and T7, were higher in June than in April.

Inferred from the biogeochemical composition of material captured in the deepest traps, we considered several possible controls on flux attenuation and so  $T_{\text{eff}}$ , such as: (a) the freshness of organic matter, indicated by the relative contribution of chlorophyll *a* to total particulate organic carbon ([POC]:[Chla]), (b) the effect of ballasting by biogenic silica ([POC]:[BSi]), (c) the lability of the particulate matter ([POC]:[PN]), and (d) the extent of zooplankton grazing on particles, indicated by the amount of pheopigments<sup>24</sup> (sum of pheophorbide-*a* and pyropheophorbide-*a* relative to Chla; [Pheo]:[Chla]) (Fig. 2). Between trap deployments, [POC]:[Chla] and [POC]:[BSi] varied considerably but did not control *Martin-b* coefficients. Molar [POC]:[PN] ratios in the deepest traps ranged from 7.7 to 10.3 but could not explain differences in export flux profiles either. Pheophorbide-*a* and pyropheophorbide-*a* are produced during zooplankton

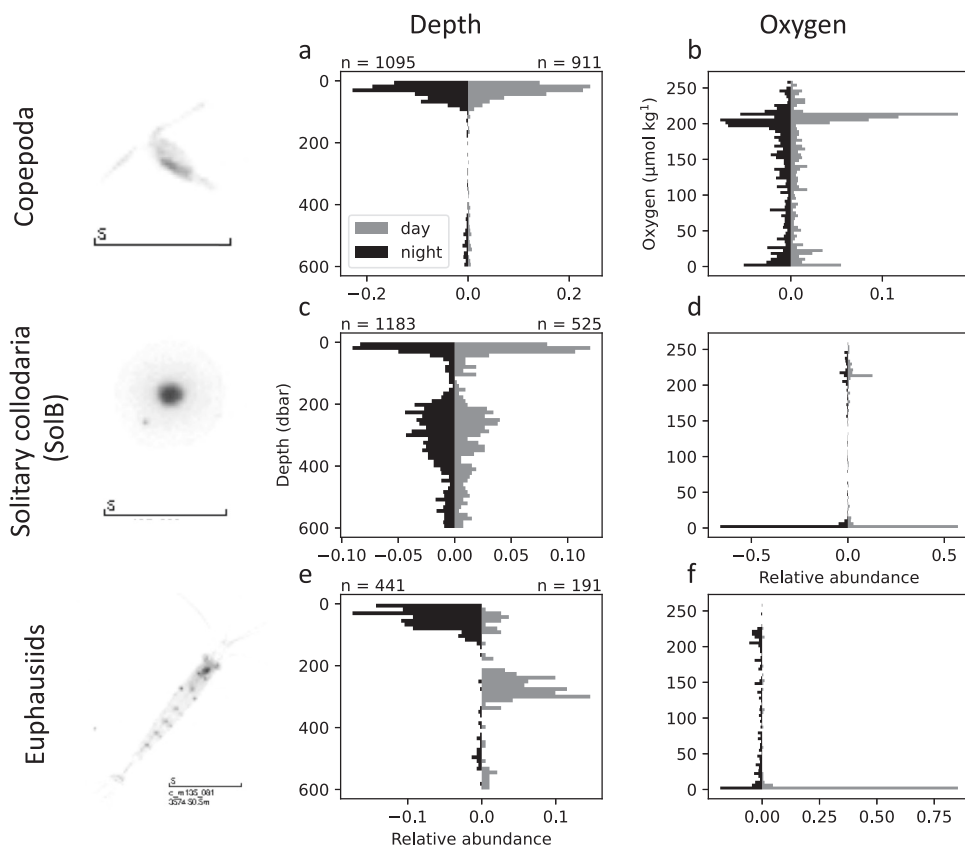


**Fig. 3 Zooplankton distribution in the OMZ.** Relative frequency distribution of copepoda (top row), solitary collodaria with a black capsule (SolB, middle row), and euphausiids (bottom row) in relation to depth (**a, c, e**) and oxygen distribution (**b, d, f**) during the day (grey bars) and night (black bars) based upon in situ images collected with an Underwater Vision Profiler (UVP5). The scale bar is always 5 mm.

degradation of *Chla* and are quantitatively the most important pigments in fecal pellets<sup>25</sup>. Pheophorbides are widely used as biomarkers for zooplankton feeding activity on sinking particles<sup>26,27</sup>. The [Pheo]:[*Chla*] ratios of the particulate material collected during this study varied between 7 and 25 [g]:[g], indicating a substantial contribution of herbivore fecal material<sup>26</sup>. Overall, carbon flux attenuation (*Martin-b*) was significantly correlated to the [Pheo]:[*Chla*] of the deepest traps ( $p < 0.01$ ;  $r = 0.81$ ;  $n = 6$ , Fig. 2f), which indicates that flux attenuation could be linked to zooplankton grazing. The [Pheo]:[*Chla*] ratio of material collected in traps above the OMZ averaged  $6.9 \pm 7.9$  and was lower than within the OMZ ( $17.3 \pm 9.3$ ) (Supplementary Fig. 2) indicating a source of feces in the OMZ rather than settling of fecal pellets out of the oxygenated surface waters. Highest [Pheo]:[*Chla*] ratio was often observed close to the upper or lower boundary of the OMZ. In the deepest traps, we measured the highest [Pheo]:[*Chla*] ratio for T7 and the lowest for T4, suggesting that particles sinking out of the OMZ had undergone the highest and lowest zooplankton reworking at these sites, respectively. (Fig. 2f, Supplementary Fig. 2). Overall, [Pheo]:[*Chla*] ratios were higher in June ( $21 \pm 11$ ) than in April ( $15 \pm 7$ ), pointing to higher grazing activity later during the season<sup>28</sup>.

Previous observations from oxygenated waters have suggested that flux attenuation correlates with the median temperature of the upper mesopelagic waters<sup>29</sup>. We therefore also compared our and previously published *b*-values using the 100 m reference depth ( $F_{100}$ ) and differentiated between low-oxygen ( $< 70 \mu\text{mol O}_2 \text{ L}^{-1}$ ) and high-oxygen ( $> 70 \mu\text{mol O}_2 \text{ L}^{-1}$ ) systems (Fig. 2d, Supplementary Table 3). Flux-attenuation in high-oxygen systems matches the prediction over a wide range of temperatures fairly well. Low-oxygen systems, however, show

large variations of *b*-values despite similar temperatures. Although *Martin-b* values at some low-oxygen sites agreed with the suggested temperature dependence, it is evident that temperature is a poor predictor of POC flux attenuation values in OMZs. One explanation for the lower-than-expected *b*-values is that hypoxia reduces particle decomposition rates as demonstrated in incubation experiments<sup>30,31</sup>, which purposefully excluded zooplankton. In the absence of larger heterotrophs, microbial decomposition of organic matter is the predominant process responsible for flux attenuation<sup>20</sup>. Indeed, *b*-values at sites with limited indications of zooplankton grazing in our study (e.g., T4) and other suboxic regions (Supplementary Table 3) are below the temperature prediction line (Fig. 2d), while flux attenuation at T7 was higher than predicted. Variations in microbial decomposition were unlikely to explain the observed large differences in carbon flux attenuation during this study since the activity of microbial hydrolytic enzymes and the bacterial biomass production in the OMZ were similar between stations<sup>21</sup>. Instead, a coherent interpretation of our biogeochemical data is that feeding activity by zooplankton tolerating low oxygen leads to higher flux attenuation.

#### Zooplankton feeding on and disrupting sinking particles.

Phaeopigment biomarkers for zooplankton grazing during this study were consistent with a microscopic analysis of sinking material caught in transparent gel-filled traps. Large phytoplankton aggregates were more frequent at T4 than at T7, while T7 showed higher abundance of large fecal pellets (Supplementary Fig. 3). Fecal pellet morphology at T7 indicated the presence of squat lobsters and euphausiids (Supplementary Fig. 4); their

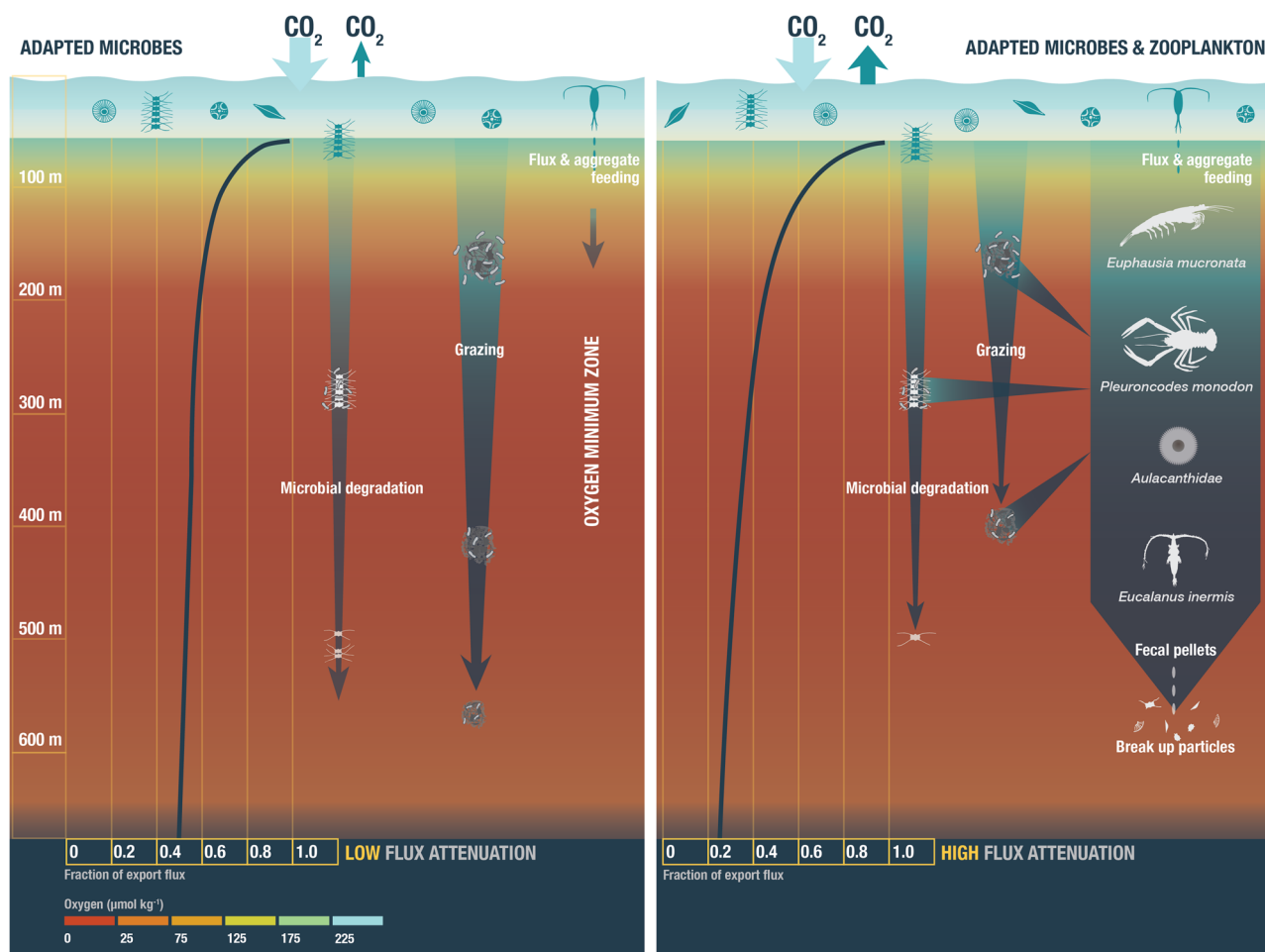


**Fig. 4 Carbon export flux attenuation in OMZs.** Conceptual model of POC export flux attenuation in the water column of OMZs. Left: Low POC flux attenuation is observed when organic matter degradation is solely driven by anaerobic microbial communities that are adapted to hypoxia. Right: In addition to anaerobic microorganisms, zooplankton that have adapted to hypoxic conditions feed on, and break up sinking particles, thereby enhancing particle flux attenuation through the OMZ.

presence in the OMZ was also confirmed by vertically stratified plankton net samples collected at the recovery sites of the traps (Supplementary Fig. 5). Both the squat lobster *Pleuroncodes monodon* and the euphausiid *Euphausia mucronata* are endemic to the Humboldt Current and perform diel vertical migrations into the OMZ core (down to 250–350 m depth approximately) during the daytime, thus tolerating hypoxia and even anoxia for prolonged periods<sup>32,33</sup>. To further resolve the fine-scale distribution patterns of zooplankton, we deployed an Underwater Vision Profiler 5 (UVP)<sup>34</sup> on the CTD-Rosette (equipped with an  $O_2$ -sensor) during both cruises (M136, and M138) as well as during an earlier cruise (M135) off Peru. 77 UVP profiles down to at least 500 m depth were analyzed. Copepod abundance showed no differences in vertical distribution between day and night, but this might be related to the taxonomic resolution attainable with the UVP, which does not allow resolution of species-specific diel vertical migration patterns (e.g., as found for *Eucalanus inermis* in the upper 200 m off Chile<sup>19</sup>). We found 88% of all copepods in the oxygenated ( $>15 \mu\text{mol kg}^{-1} O_2$ ) surface layer (Fig. 3a, b), 0.1% were found below the OMZ at  $O_2$  concentrations  $>15 \mu\text{mol kg}^{-1} O_2$ , 7% were found at the upper and lower oxycline at oxygen concentrations between 4 and  $15 \mu\text{mol kg}^{-1}$  and 5% were found in the OMZ at  $O_2$  concentrations below  $4 \mu\text{mol kg}^{-1}$ . Overall, copepods seem to avoid the OMZ, but some species such as *Eucalanus inermis* may use it as a diapause refuge, others as feeding ground<sup>35</sup>. In situ imaging also indicated the presence of

several giant rhizaria taxa in the OMZ off Peru (Fig. 3c, d; Supplementary Fig. 6). Importantly, large parts of the rhizaria populations were found at oxygen concentrations of  $<4 \mu\text{mol kg}^{-1}$  during both day- and night-time (Fig. 3d; Supplementary Fig. 6b, d, f). In total, 63% of the solitary black collodarians (SolB) were found in the core of the OMZ at  $<4 \mu\text{mol } O_2 \text{ kg}^{-1}$ , 7% between 4 and  $15 \mu\text{mol } O_2 \text{ kg}^{-1}$  and 30% at  $>15 \mu\text{mol } O_2 \text{ kg}^{-1}$  (Fig. 3c). The solitary globular collodarians (SolG) and *Aulosphaeridae* were more evenly distributed (Supplementary Fig. 6c) and the *Aulacantha* showed a slight preference for the upper and lower oxycline (Supplementary Fig. 6e). However, also in these three groups 64, 60 and 41% of all imaged organisms, respectively, were found at  $<4 \mu\text{mol } O_2 \text{ kg}^{-1}$ . Euphausiids were observed in the anoxic core (200–400 m) of the OMZ during the daytime and in the upper water column during the night (Fig. 3a, b; Supplementary Figs. 4 and 5). Although we cannot directly correlate the presence of rhizaria or euphausiids to our flux attenuation values, as the data do not stem from parallel deployments, the overall high presence of flux-feeding rhizaria<sup>36</sup> within the OMZ and the presence of krill at the upper oxycline strongly suggest zooplankton interacting with and grazing on sinking particles at extremely low oxygen levels off Peru. Crustaceans, especially large krill and *Pleuroncodes* may contribute to flux attenuation via direct grazing on sinking phytoplankton cells and marine snow, and also via disruption of large aggregates<sup>37</sup>. Off California, *Euphausia pacifica* abundances of

5–10 ind. m<sup>-3</sup> resulted in a net increase of aggregate numbers, likely via the fragmentation of larger aggregates into smaller ones<sup>38</sup>. At T7 we found krill abundances of 6 ind. m<sup>-3</sup> at the lower oxycline during the night (Supplementary Fig. 5). In the Humboldt current system, dense krill swarms can host up to 50 ind. m<sup>-3</sup> off Chile<sup>18</sup>, and we found up to 90 ind. m<sup>-3</sup> off Peru. Dense zooplankton aggregations may also disrupt sinking particles during their diel migrations to and from their daytime residence depth of about at 200–400 m.

**Potential limitations of zooplankton effects on BCP under hypoxia.** Our results highlight the importance of hypoxia-adapted zooplankton in explaining variations of the BCP in OMZs underlying highly productive waters such as the Humboldt current system. Here, pelagic crustaceans and other zooplankton species might exploit and transform particles rapidly, in contrast to microbes that grow slowly under anoxic conditions<sup>20,21</sup> and cannot efficiently attenuate the flux of rapidly sinking particles (Fig. 4). To date, little is known about the foraging activities of zooplankton in the OMZ<sup>18,39</sup>. An important conclusion of our study is that behavioral and physiological adaptations of zooplankton to environmental extremes are critical, but largely neglected, traits for understanding the BCP. The Humboldt coastal upwelling system is generated by ocean circulation and has exhibited permanent hypoxia since >14.7 ka with little fluctuation<sup>40</sup>. Sustained by abundant nutrients, the production and supply of organic matter to the deeper hypoxic waters have always been high, creating an environment rich in food and low in competition, thus particularly rewarding for heterotrophs that can tolerate low-oxygen conditions. In this sense, ‘old’ OMZ ecosystems like the Humboldt Current may be unique in that they have allowed the proliferation of zooplankton specifically adapted to hypoxia. In systems that have recently suffered from oxygen deficiency due to eutrophication and climate warming, zooplankton tend to avoid hypoxic layers<sup>41</sup>. On the other hand, opportunistic zooplankton species may be able to exploit even transient hypoxia, as recently demonstrated by the mass occurrence of the gelatinous, flux-feeding polychaete *Poebius sp.*, in ‘dead zone’ eddies of the Tropical North Atlantic<sup>42</sup>. Predicting the impacts of zooplankton on CO<sub>2</sub> sequestration in the ocean is challenging due to the high temporal and spatial heterogeneity of organismal abundance and distribution. Even where zooplankton have adapted to hypoxia, the distribution of these metazoans is not uniform. Zooplankton aggregate in patches is often associated with submesoscale (~10<sup>3</sup>–10<sup>4</sup> m) and mesoscale (~10<sup>4</sup>–10<sup>5</sup> m) hydrographical features<sup>43</sup>. Patchiness of zooplankton abundance can also be an explanation for the observed range of [Pheo]:[Chl<sub>a</sub>] in the trap material and the corresponding variability in POC flux attenuation during this study, where meso- and submesoscale physical variability due to filaments and eddies is typically high<sup>44</sup>. Moreover, species-specific traits related to metabolic adaptations and acclimations, life cycle dynamics, and behavior are further components of the complex ecology of mesopelagic organisms. Overall, the patchy distribution and the various roles of mesopelagic organisms on flux attenuation and generation<sup>39</sup> limit, if not prohibit, simplified empirical approaches to estimate carbon export fluxes from physical and chemical environmental data alone<sup>45,46</sup>. Based on several independent methods, our results provide consistent evidence that zooplankton interact with and substantially reduce particle export fluxes in low-oxygen systems. Our study supports the emerging perception of zooplankton as gatekeepers<sup>39</sup> of the biological carbon pump, even within the OMZ. Given the potentially significant influence of planktonic fauna on the BCP, we argue that observations and knowledge of mesopelagic ecosystem dynamics

must be greatly expanded to make reliable predictions about the marine carbon cycle.

## Methods

**Study site and sample collection.** Samples were collected in April and June 2017 during the RV *Meteor* cruises M136 and M138 off Peru. Details on the hydrography and O<sub>2</sub> concentrations in the study region during sampling are given elsewhere<sup>21</sup>. We collected sinking particles using surface-tethered sediment traps<sup>47,48</sup> at six locations (Supplementary Fig. 1, Supplementary Table 1). Sediment traps were deployed for two to six days and collected particles at eight depths (Supplementary Table 1) between 50 and 600 m in the open ocean (T1, T3, T4, T6, and T7), and 5 depths between 40 and 300 m on the shelf (T2). One trap array (T5) was lost during the deployment. The first trap depth was always chosen below the base of the mixed layer based on CTD profiles. At each depth, twelve acrylic particle interceptor tubes (PITs) mounted in a PVC cross-frame were deployed. Each PIT was equipped with an acrylic baffle at the top to minimize the collection of swimmers<sup>47,48</sup>. The PITs were 7 cm in diameter and 53 cm in height with an aspect ratio of 7.5 and a collection area of 0.0038 m<sup>2</sup>. The cross-frame and PITs were attached to a line with a bottom weight and a set of surface and subsurface floats. The procedures for PIT preparation and sample recovery followed Engel et al.<sup>48</sup>. Samples were split into aliquots that were processed for the different biogeochemical analyses. At selected traps, we collected intact individual particles in situ using gel cups, i.e., cylindrical collectors placed at the bottom of the PIT tubes (collection area of 0.0020 m<sup>2</sup>) and filled with polyacrylamide gels<sup>49</sup>. For T4 and T7, those gel cups were placed at 200, 300, 400, 500, and 600 m depth. Following recovery, gel cups were placed under a Zeiss® Stemi 508 stereomicroscope coupled to a Zeiss® Axiocam ERc 5 s digital camera. Gels were then photographed at a magnification of 6.5 against a laser-etched glass grid (each cell of 14 by 12.5 mm)<sup>49</sup>, using the Zen lite software provided by Zeiss®. A specifically designed light system providing a homogeneous source of light from below the gels was used to avoid any shading on the photographs. We assessed the flux abundance of various types of particles in both traps 4 and 7 following methods presented in Ebersbach and Trull<sup>50</sup>. We grouped observed particles into distinct categories: phytoplankton aggregates (PAGG), fecal aggregates (FAGG), and various fecal pellets (FP), including cylindrical, oval, and spherical fecal pellets. The flux abundance spectra of each type of particle at both traps 4 and 7 were then binned into five size classes in equivalent spherical diameter (ESD): 0.071–0.145, 0.145–0.296, 0.296–0.603, 0.603–1.228, >1.228 mm ESD, shown in Supplementary Fig. 3.

An underwater vision profiler (UVP5) was mounted in the CTD rosette frame throughout the cruises to obtain high-resolution particle abundance and size spectra data as well as zooplankton images<sup>34</sup>. At the sites of traps 6 and 7, depth-stratified zooplankton samples were collected by day/night vertical haul pairs (1 m s<sup>-1</sup>) with a Hydrobios Multinet Midi (0.25 m<sup>2</sup> mouth opening, 5 nets, 200 μm mesh). Samples were rinsed into Kautex® jars and fixed in 4% borax-buffered formaldehyde in seawater solution. Samples were scanned on an Epson Perfection V750 Pro scanner in a modification of the ZooScan method<sup>51</sup>. Both the UVP5 and the ZooScan image dataset were uploaded to Ecotaxa<sup>34</sup> (<http://ecotaxa.obs-vlfr.fr/>) and predicted into different classes using the in-built random forest algorithm with deep learning features. Automated image sorting was then manually validated by experts. Biomass was estimated according to Lehet and Hernández-León<sup>52</sup>. Rhizaria categories were distinguished according to Biard et al.<sup>53</sup>. The solitary black collodarians (SolB, Fig. 2) are large spherical

organisms with a dense central part (black/dark). The solitary globular colloidarians (SolGlob, Supplementary Fig. 6) are large, spherical to-oval organisms with a homogenous grey (or dark-grey) surface. The central sphere is surrounded by a blurry halo generated by a network of pseudopodial extensions.

**Biogeochemical analysis.** Particulate organic carbon (POC), nitrogen (PN), and pigments were determined by filtering aliquots, of 100 to 200 mL of the trapped material onto pre-combusted GF/F filters (8 h at 500 °C) at low vacuum (< 200 mbar). POC and PN samples were filtered in triplicate, and pigments in duplicate. Filters for POC-PN were stored dry, acid-fumed (37% hydrochloric acid) to remove carbonates, and dried for 12 h at 60 °C before analysis. POC and PN were determined with an elemental analyzer (Euro EA, Hechatech). Biogenic silica (BSi) was determined in aliquots of 50 to 100 mL, filtered in duplicate onto 0.4 µm cellulose acetate filters. Samples were stored at -20 °C until analysis. For the measurements, filters were digested in NaOH at 85 °C for 135 min; the pH was adjusted to 8 with HCl. Silicate was measured spectrophotometrically<sup>54</sup>. Pigments were extracted with 90% acetone and homogenized with glass beads. The tube containing the filter was centrifuged for 10 min at 5000 rpm, and the supernatant was collected. Extracts were filtered through 0.2 µm Teflon filters and stored at -80 °C until analysis. Chlorophylls (chlorophyll *a*, pheophytin *a*, pheophorbide *a*, and pyropheophorbide *a*) were determined using reverse-phase High-Performance Liquid Chromatography (HPLC, DionexUlti Mate R 3000LC system equipped with an autosampler, a photodiode array and a fluorescence detector, ThermoScientific). Pigments were identified by using a comparison of their retention times and spectral properties with standards (DHI Water & Environment, Denmark). Data fits and statistical tests were performed with the software packages Microsoft Office Excel 2019 and Sigma Plot 14.0 (Systat).

**Reporting summary.** Further information on research design is available in the Nature Portfolio Reporting Summary linked to this article.

### Data availability

All data included in this study are publicly available. Engel, Anja; Cisternas-Novoa, Carolina; Hauss, Helena; Kiko, Rainer; Le Moigne, Frédéric A C: Biological carbon pump efficiency in the Humboldt current system off Peru: sediment traps during METEOR cruises M136 and M138. PANGAEA, <https://doi.pangaea.de/10.1594/PANGAEA.963289>.

Received: 24 October 2023; Accepted: 22 November 2023;

Published online: 06 December 2023

### References

- Volk, T. & Hoffert, M. Ocean carbon pumps: analysis of relative strengths and efficiencies in ocean-driven atmospheric CO<sub>2</sub> changes. (eds E. Sundquist and W. S. Broecker) *The Carbon Cycle And Atmospheric CO<sub>2</sub>: Natural Variations Archean To Present* (AGU, Washington, DC, 1985), 99–110.
- Parekh, P., Dutkiewicz, S., Follows, M. J. & Ito, T. Atmospheric carbon dioxide in a less dusty world. *Geophys. Res. Lett.* **33**, L03610 (2006).
- Kwon, E., Primeau, F. & Sarmiento, J. The impact of remineralisation depth on the air–sea carbon balance. *Nat. Geosci.* **2**, 630–635 (2009).
- Buesseler, K. O., Boyd, P. W., Black, E. E. & Siegel, D. A. Metrics that matter for assessing the ocean biological carbon pump. *Proc. Natl Acad. Sci. USA* **117**, 9679–9687 (2020).
- Martin, J. H., Knauer, G. A., Karl, D. M. & Broenkow, W. W. Vertex—carbon cycling in the Pacific. *Deep Sea Res. A* **34**, 267–285 (1987).
- De la Rocha, C. & Passow, U. Factors influencing the sinking of POC and the efficiency of the biological carbon pump. *Deep Sea Res. II* **54**, 639–658 (2007).
- Henson, S. A., Le Moigne, F. A. C. & Giering, S. L. C. Drivers of carbon export efficiency in the global ocean. *Glob. Biogeochem. Cycles* **33**, 891–903 (2019).
- Stramma, L., Johnson, G. C., Sprintall, J. & Mohrholz, V. Expanding oxygen minimum zones in the tropical ocean. *Science* **320**, 655–658 (2008).
- Jahnke, R. A. A global synthesis. Carbon and nutrient fluxes in continental margins: a global synthesis. In: (eds Liu, K. K., Atkinson, L., Quinones, R., Talaue-McManus, L.) *Global Change: The IGBP Series*. (Springer-Verlag, 2010).
- Lam, P. & Kuypers, M. M. M. Microbial nitrogen cycling processes in oxygen minimum zones. *Annu. Rev. Mar. Sci.* **3**, 317–348 (2011).
- Wright, J. J., Konwar, K. M. & Hallam, S. J. Microbial ecology of expanding oxygen minimum zones. *Nat. Rev. Microbiol.* **10**, 381–394 (2012).
- Engel, A., Kiko, R. & Dengler, M. Organic matter supply and utilization in oxygen minimum zones. *Ann. Rev. of Mar. Sci.* **14**, 355–378 (2022).
- Bretagnon, M., Paulmier, A., Garçon, V. & Dewitte, B. Modulation of the vertical particle transfer efficiency in the oxygen minimum zone off Peru. *Biogeosciences* **15**, 5093–5111 (2018).
- Devol, A. H. & Harnett, H. E. Role of the oxygen minimum zone in transfer of organic carbon to the deep ocean. *Limnol. Oceanogr.* **25**, 1684–1690 (2001).
- Tutasi, P. & Escribano, R. Zooplankton diel vertical migration and downward C flux into the oxygen minimum zone in the highly productive upwelling region off northern Chile. *Biogeosciences* **17**, 455–473 (2020).
- Fuenzalida, R., Schneider, W., Garcés-Vargas, J., Bravo, L. & Lange, C. Vertical and horizontal extension of the oxygen minimum zone in the eastern South Pacific Ocean. *Deep Sea Res. II* **56**, 992–1003 (2009).
- Wishner, K. F. et al. Ocean deoxygenation and zooplankton: very small oxygen differences matter. *Sci. Adv.* **4**, eaau5180 (2018).
- Antezana, T. Adaptive behavior of *Euphausia mucronata* in relation to the oxygen minimum layer of the Humboldt Current. *Oceanogr. East. Pac.* **2**, 29–40 (2002).
- Escribano, R., Hidalgo, P. & Krautz, C. Zooplankton associated with the oxygen minimum zone system in the northern upwelling region of Chile during March 2000. *Deep Sea Res. II* **56**, 1083–1094 (2009).
- Cavan, E. L., Trimmer, M., Shelley, F. & Sanders, R. Remineralization of particulate organic carbon in an ocean oxygen minimum zone. *Nat. Commun.* **8**, 14847 (2017).
- Maßmig, M., Lüdke, J., Krahnemann, G. & Engel, A. Bacterial degradation activity in the eastern tropical South Pacific oxygen minimum zone. *Biogeosciences* **17**, 215–230 (2020).
- Kavelage, T. et al. Aerobic microbial respiration in oceanic oxygen minimum zones. *PLoS ONE* **10**, e0133526 (2016).
- Behrenfeld, M. J. & Falkowski, P. G. Photosynthetic rates derived from satellite-based chlorophyll concentration. *Limnol. Oceanogr.* **42**, 1–20 (1997).
- Welschmeyer, N. A. & Lorenzen, C. J. Chlorophyll budgets: Zooplankton grazing and phytoplankton growth in a temperate fjord and the Central Pacific ‘Gyres’. *Limnol. Oceanogr.* **30**, 1–21 (1985).
- Goericke, R., Strom, S. L. & Bell, M. A. Distribution and sources of cyclic pheophorbides in the marine environment. *Limnol. Oceanogr.* **45**, 200–211 (2000).
- Stukel, M. R. et al. Sinking carbon, nitrogen, and pigment flux within and beneath the euphotic zone in the oligotrophic, open-ocean Gulf of Mexico. *J. Plankton Res.* **44**, 711–727 (2022).
- Wakeham, S. G. et al. Organic biomarkers in the twilight zone—time series and settling velocity sediment traps during MedFlux. *Deep Sea Res. II* **56**, 1437–1453 (2009).
- Taylor, G. T. et al. Ecosystem responses in the southern Caribbean Sea to global climate change. *Proc. Natl Acad. Sci. USA* **109**, 19315–19320 (2012).
- Marsay, C. M. et al. Attenuation of sinking particulate organic carbon flux through the mesopelagic ocean. *Proc. Natl Acad. Sci. USA* **112**, 1089–1094 (2015).
- Le Moigne, F. A. C. et al. On the effect of low oxygen concentrations on bacterial degradation of sinking particles. *Sci. Rep.* **7**, 16722 (2017). Art. No.
- Van Mooy, B. A. S., Keil, R. G. & Devol, A. H. Impact of suboxia on sinking particulate organic carbon: enhanced carbon flux and preferential degradation of amino acids via denitrification. *Geochim. Cosmochim. Acta* **66**, 457–465 (2002).
- Kiko, R. et al. The squat lobster *Pleuroncodes monodon* tolerates anoxic “dead zone” conditions off Peru. *Mar. Biol.* **162**, 1913–1921 (2015).
- Kiko, R. & Hauss, H. On the estimation of zooplankton-mediated active fluxes in Oxygen Minimum Zone regions. *Front. Mar. Sci.* **6**, 741 (2019).
- Picheral, M. et al. The Underwater Vision Profiler 5: an advanced instrument for high spatial resolution studies of particle size spectra and zooplankton. *Limnol. Oceanogr. Methods* **8**, 462–473 (2010).
- Wishner, K. F., Seibel, B. & Outram, D. Ocean deoxygenation and copepods: coping with oxygen minimum zone variability. *Biogeosciences* **17**, 2315–2339 (2020).
- Biard, T. & Ohman, M. D. Vertical niche definition of test-bearing protists (*Rhizaria*) into the twilight zone revealed by in situ imaging. *Limnol. Oceanogr.* **65**, 2583–2602 (2020).

37. Briggs, N., Dall’Omo, G. & Claustre, H. Major role of particle fragmentation in regulating biological sequestration of CO<sub>2</sub> by the oceans. *Science* **367**, 791–793 (2020).
38. Dilling, L. & Allredge, A. L. Fragmentation of marine snow by swimming macrozooplankton: a new process impacting carbon cycling in the sea. *Deep Sea Res. I* **47**, 1227–1245 (2000).
39. Stukel, M. R., Ohman, M. D., Kelly, T. B. & Biard, T. The roles of suspension-feeding and flux-feeding zooplankton as gatekeepers of particle flux into the mesopelagic ocean in the northeast Pacific. *Front. Mar. Sci.* **6**, 397 (2019).
40. Moffitt, S. E. et al. Paleoceanographic Insights on recent oxygen minimum zone expansion: lessons for modern oceanography. *PLoS ONE* **10**, e0115246 (2015).
41. Roman, M. R. et al. Impacts of hypoxia on zooplankton spatial distributions in the northern Gulf of Mexico. *Estuar. Coasts* **35**, 1261–1269 (2012).
42. Christiansen, S. et al. Particulate matter flux interception in oceanic mesoscale eddies by the polychaete *Poecobius* sp. *Limnol. Oceanogr.* **63**, 2093–2109 (2018).
43. Bertrand, A. et al. Broad impacts of fine-scale dynamics on seascape structure from zooplankton to seabirds. *Nat. Commun.* **5**, 5239 (2014).
44. Thomsen, S. et al. Do submesoscale frontal processes ventilate the oxygen minimum zone off Peru? *Geophys. Res. Lett.* **43**, S367–S386 (2016).
45. Laufkötter, C. et al. Temperature and oxygen dependence of the remineralization of organic matter. *Glob. Biogeochem. Cycl.* **31**, 1038–1050 (2017).
46. Henson, S. A. et al. A reduced estimate of the strength of the ‘ocean’s biological carbon pump. *Geophys. Res. Lett.* **38**, L04606 (2011).
47. Knauer, G. A., Martin, J. H. & Bruland, K. W. Fluxes of particulate carbon, nitrogen, and phosphorus in the upper water column of the northeast Pacific. *Deep Sea Res.* **26**, 97–108 (1979).
48. Engel, A., Wagner, H., Le Moigne, F. A. C. & Wilson, S. T. Particle export fluxes to the oxygen minimum zone of the Eastern Tropical North Atlantic. *Biogeosciences* **14**, 1825–1838 (2017).
49. Lundsgaard, C. Use of a high viscosity medium in studies of aggregates. In: *Sediment Trap Studies in the Nordic Countries. 3. Proceeding of the Symposium on Seasonal Dynamics of Planktonic Ecosystems and Sedimentation in Coastal Nordic Waters*. Finnish Environment Agency, 141–152 (1995).
50. Ebersbach, F. & Trull, T. W. Sinking particle properties from polyacrylamide gels during the Kerguelen Ocean and Plateau compared study (KEOPS): zooplankton control of carbon export in an area of persistent natural iron inputs in the Southern Ocean. *Limnol. Oceanogr.* **53**, 212–224 (2008).
51. Gorsky, G. et al. Digital zooplankton image analysis using the ZooScan integrated system. *J. Plankton Res.* **32**, 285–303 (2010).
52. Lehette, P. & Hernández-León, S. Zooplankton biomass estimation from digitized images: a comparison between subtropical and Antarctic organisms. *Limnol. Oceanogr. Methods* **7**, 304–308 (2009).
53. Biard, T. et al. In situ imaging reveals the biomass of giant protists in the global ocean. *Nature* **532**, 504–507 (2016).
54. Hansen, H. P. & Koroleff F. Determination of nutrients. In *Methods Seawater Anal* 3rd edn, 159–228 (1999).

## Acknowledgements

Jon Roa, Tania Klüver, Marie Massmig, Ruth Flerus, Kerstin Nachtigall, Claudia Sforza, and Christian Begler supported trap preparation, deployments, sampling, or sample analysis. This research was supported by the Helmholtz Association, the DFG Collaborative Research Center 754 ‘Climate-Biogeochemistry Interactions in the Tropical

‘Ocean’ (B9; grant/award no. 27542298), the collaborative project CUSCO—Coastal Upwelling System in a Changing Ocean (grant no. 03F0813D) of the German Federal Ministry of Education and Research (BMBF) and by a Fellowship of the Excellence Cluster ‘The Future ‘Ocean’ (CP1403 to F.A.C.L.M.) funded by the DFG. RK acknowledges support via a ‘Make Our Planet Great Again’ grant of the French National Research Agency within the ‘Program d’Investissements d’Avenir’; reference ‘ANR-19-MPGA-0012’. We thank the crew, officers, and captains of the F.S. Meteor as well as the scientific parties of cruises M135, M136, and M138. H.H. acknowledges financial support by the Bundesministerium für Bildung und Forschung (BMBF) through the project CO2Meso (03F0876A).

## Author contributions

A.E., C.C.N., and F.A.C.L.M. designed the study. C.C.N. and F.A.C.L.M. performed trap deployments at sea, and biogeochemical, and microscopic analysis. H.H. and R.K. were in charge of the UVP5 operation and zooplankton sampling. All authors analyzed the data. A.E. wrote the initial draft of the paper and C.C.N., F.A.C.L.M., H.H., and R.K. edited subsequent drafts.

## Funding

Open Access funding enabled and organized by Projekt DEAL.

## Competing interests

The authors declare no competing interests.

## Additional information

**Supplementary information** The online version contains supplementary material available at <https://doi.org/10.1038/s43247-023-01140-6>.

**Correspondence** and requests for materials should be addressed to Anja Engel.

**Peer review information** *Communications Earth & Environment* thanks the anonymous reviewers for their contribution to the peer review of this work. Primary Handling Editors: Clare Davis. A peer review file is available.

**Reprints and permission information** is available at <http://www.nature.com/reprints>

**Publisher’s note** Springer Nature remains neutral with regard to jurisdictional claims in published maps and institutional affiliations.



**Open Access** This article is licensed under a Creative Commons Attribution 4.0 International License, which permits use, sharing, adaptation, distribution and reproduction in any medium or format, as long as you give appropriate credit to the original author(s) and the source, provide a link to the Creative Commons licence, and indicate if changes were made. The images or other third party material in this article are included in the article’s Creative Commons licence, unless indicated otherwise in a credit line to the material. If material is not included in the article’s Creative Commons licence and your intended use is not permitted by statutory regulation or exceeds the permitted use, you will need to obtain permission directly from the copyright holder. To view a copy of this licence, visit <http://creativecommons.org/licenses/by/4.0/>.

© The Author(s) 2023